Experimental adaptive-optics system for Big Solar Vacuum Telescope. II. Efficiency of stabilization of a solar disk fragment image on the entrance slit of a spectrograph

L.V. Antoshkin, N.N. Botygina, O.N. Emaleev, L.N. Lavrinova, V.P. Lukin, A.I. Petrov, B.V. Fortes, and A.P. Yankov

Institute of Atmospheric Optics,
Siberian Branch of the Russian Academy of Sciences, Tomsk

Received December 3, 1999

The efficiency of an experimental adaptive-optics system is studied as applied to stabilization a solar disk fragment image on the entrance slit of a spectrograph. The studies were performed at the Big Solar Vacuum Telescope of the Institute of Solar–Terrestrial Physics SB RAS. Depending on the atmospheric conditions, the variance of image jitter on the spectrograph slit was reduced by a factor from 16 to 40 when applying the adaptive-optics system. The relative error of regulation did not exceed 25%. The harmonics of the image displacement signal at the frequencies of 0 to 30 Hz were effectively suppressed.

Introduction

Specialists from the Institute of Solar-Terrestrial Physics SB RAS have designed a unique instrument[1] with high spatial and spectral resolution for studying processes on the Sun by spectral methods. It is based on the Big Solar Vacuum Telescope (BSVT) and a spectrograph. However, the jitter of the solar disk image due to atmospheric turbulence and vibrations of the telescope frame affects the quality of spectrograms recorded with this instrument.

For stabilization of an image fragment on the entrance slit of the spectrograph, we have developed and tested a pilot tracking system with a quadrant receiver and a tilt-controlled mirror.

The use of a tracking system with a quadrant receiver imposes some restrictions on the areas of the solar disk, studied since the system can operate with only such image fragments, which include a pronounced local inhomogeneity in the illumination distribution. The proposed adaptive system was test-operated for stabilization of a fragment of the solar disk image in the vicinity of a solar pore. The researchers place special value on the studies of the processes proceeding in this area.

Experimental setup

The experimental setup is schematically shown in Fig. 1. A bimorphous deflector 36 mm in diameter was used as a controlled mirror. The deflector was designed and manufactured at the Laboratory of Applied and Adaptive Optics of the IAO. It has been test-operated in an actual adaptive-optics system.[2,3] The deflector was set in front of the telescope focus 280 cm far from the focal plane and took part in formation of an image on the spectrograph slit. The deflector sensitivity was $1.2 \cdot 10^{-6}$ rad/V. The resonance frequency of the mirror depended on the support the mirror is fastened to and on the fastening method; in this system it was roughly 120 Hz.

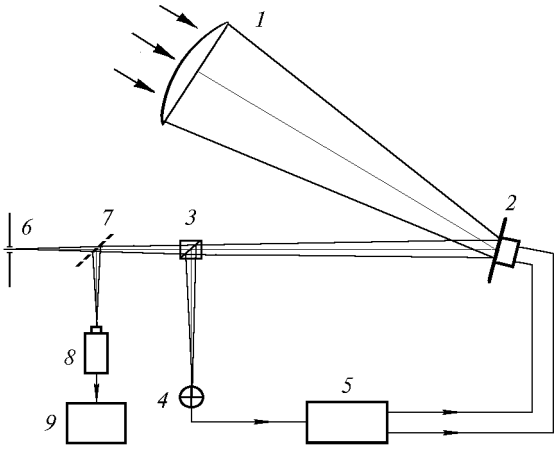

Fig. 1. Experimental setup: objective *1* of the telescope (760 mm in diameter and 40 m focal length), controlled mirror *2*, beam-splitting cube *3*, receiving device *4*, control unit *5*, entrance slit of the spectrograph *6*, mirror for optical control of image stabilization quality *7*, video camera *8*, and a computer *9*.

A beam-splitting cube was set between the controlled mirror and the entrance slit. It directed a portion of the beam to the entrance of the receiving

system. The receiving system consisted of an optical system for image scaling, an FDK–142 quadrant receiver, and amplifiers of the output signals from the receiver. The receiver center, as well as the spectrograph slit center, are on the optical axis in the telescope focal plane. Signals from the amplifiers came to two identical *X* and *Y* channels of the control unit *5* via the bimorphous deflector.

The electronic unit of the tracking system with the feedback via the optical channel is schematically shown in Fig. 2.

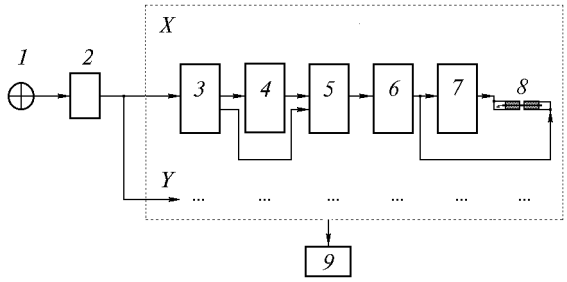

Fig. 2. Electronic unit of the tracking system: FDK–142 quadrant photodetector *1*, input amplifiers *2*, unit for calculation of image displacement *3*, displacement memory unit *4*, unit for calculation of the control signal *5*, high-voltage amplifiers *6* and *7*, piezoelectric deflector *8*, and computer *9*.

The system employs the following control algorithm:

– the unit for calculation of the displacement of a solar pore image generates signals of image displacement in the coordinate system set by the quadrant receiver;

– the displacement memory unit memorizes the required position of the image on the receiver;

– the unit for calculation of the control signal determines the error signal and generates control signals;

– the control signals are transformed by high-voltage amplifiers and are applied to the plates of the piezoelectric deflector. The maximum signal amplitude at the amplifier output is 300 V.

Under the action of these signals, the controlled mirror changes its tilt, thus stabilizing the image position on the receiver and on the spectrograph entrance slit.

The system can be operated in two modes: as a null device and in the mode of memorizing the initial position and stabilizing the image in this position.

Signals from any system unit are processed with a computer. For this purpose, the specialized software/hardware system "Signal analyzer" has been developed.[4] It includes a personal computer, an 8-channel analog input system, and a 12-bit ADC.

The efficiency of the tracking system by the quality of stabilization of an image fragment on the spectrograph slit was evaluated using a video camera (see Fig. 1), the image from which was entered into the personal computer.

Results and discussion

The efficiency of the adaptive-optics system for image stabilization was evaluated in several ways:

1. The relative error of tracking along the coordinate *X* and the coordinate *Y* was determined as the ratio of the rms deviation of the error signal to the rms deviation of the image displacement signal at the open control loop.

2. With the use of video information entered and processed in the computer, the ratio of the variances of image centroid displacements for the image including a solar pore without and with the image stabilization on the spectrograph entrance slit was calculated.

3. For characterizing the dynamic properties of the tracking system, the ratios $\mu(f) = N_1(f)/N_2(f)$ and $\eta(f) = [N_1(f) - N_2(f)]/N_1(f)$ were calculated, where $N_1(f)$ and $N_2(f)$ are the spectral power density of the image displacement signal in the system without and with the image stabilization on the spectrograph slit after averaging over ten realizations each 1.28 s long.

To determine the relative error of tracking, the histograms of 60-s realizations of the image displacement signals were collected. The histograms were recorded sequentially at sampling time of several seconds in the tracking mode and at the open control loop. The signal quantification frequency was 400 Hz with the quantification step of 2.44 mV. The measurements were conducted under clear sky conditions at different wind velocity and time. The image of the solar pore, which was tracked by the system, was 5 mm in size. The field of view of the receiving system (0.34 mrad) did not exceed the angular scale of correlation of the wave front tilts of the incident radiation [0.45 mrad (Ref. 5)].

Depending on the measurement conditions, the relative error of tracking varied from 0.15 to 0.25. The minimum observation error was observed in the channel *X* (the axis *X* was directed along the spectrograph slit) in the first half of a day at the northerly wind with the speed about 10 m/s. Under these conditions and open control loop the variance of image jitter along the slit was maximum being several times larger than the variance of the image jitter in the crosswise direction.

Image jitter on the spectrograph entrance slit was recorded simultaneously with the histograms by a standard video camera, and the image was visualized on a monitor. Thus, the quality of the image stabilization was optically checked. The video frames of the recorded realizations were processed in the computer, and the processed results showed that the variance of the residual displacements of the centroid of the solar pore image did not exceed 1/16 of the variance of the displacements of the image centroid at the open control loop.

To illustrate the dynamic peculiarities of the tracking system, Fig. 3 shows the power spectra of the image displacement signals at the open control loop and after the tracking system was turned on. Signal

realizations were recorded at 11:00 L.T. at the northerly wind of 7 m/s and air temperature of 14°C. The appearance of a high-frequency error signal in the spectrum is caused by the resonance of the controlled mirror. However, as is seen from the figure, the variance of the image displacement signal at these frequencies is about 1/150 of the variance of the image displacement signal in the system without control over wave front tilts, i.e., the control system introduces insignificant noise at the resonance frequency. The frequency dependence of the degree of the harmonics suppression in the image jitter spectrum (Fig. 3*a*) is shown as functions $\mu(f)$ and $\eta(f)$ in Fig. 4.

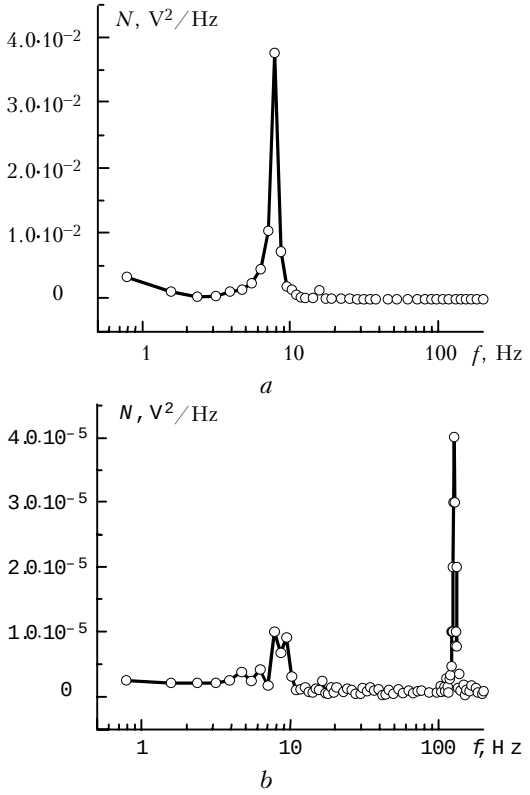

Fig. 3. Power spectra of the image displacement signals along the spectrograph entrance slit: at open control loop (*a*) and at the image stabilization on (*b*).

Similar processing of realizations recorded at different time at the northerly and southerly winds of 3 to 10 m/s speed and air temperature from 14 to 20°C in August 1999 showed that the main contribution to the image displacement signal came from the harmonics at the frequencies lower than 30 Hz, in response to which the tracking system acted quite effectively. The efficiency of the adaptive system, which is determined by the function $\eta(f)$, at strong image jitter proved to be higher than 0.9 at the frequency from 0 to 30 Hz (Fig. 4*b*). At the same time, in some realizations at a strong wind the signal was cut, that is, the system operated at limiting regulation in response to the output voltage of high-voltage amplifiers.

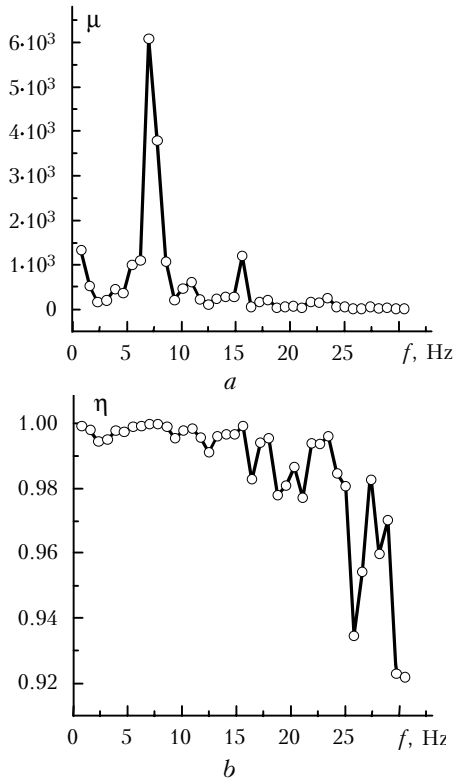

Fig. 4. Efficiency of the image stabilization system: frequency dependence of the ratio of spectral power densities of image displacement signal at open and closed control loop (*a*); frequency dependence of the degree of suppression of the image jitter on the spectrograph entrance slit (*b*).

The efficiency of the system in the mode providing for memorizing the initial position of the image and image stabilization at the initial position turned out to be higher than in the null device operation mode, that is, in the mode of image stabilization in the position at which the difference of the signals from the top and bottom, left and right quadrants of the receiver is equal to zero. This is likely connected with the fact that the system tracked the image fragment surrounded by inhomogeneously illuminated region around the pore image.

Analyzing the spectra of signals recorded under different conditions, we noticed that in the first half of a day the image mostly displaced along the spectrograph slit (axis *X* of the system), while in the second half of a day the total variance of the image jitter decreased, but displacements across the slit prevailed.

Figure 5*a* shows the power spectra of signals recorded since 11:01 and since 18:24 L.T. The maximum of the spectral power density was observed at the frequency of 7.8 Hz. The signal spectrum recorded in the first half of the day included the harmonic at the doubled maximum frequency. We assumed that vibrations of telescope elements caused this jitter: vibrations of the siderostat mirror about the horizontal axis. It was checked that the control over mirror tilts

about this axis at roughly 11:00 L.T. led to prevailing image displacements along the spectrograph slit. At roughly 18:00 L.T., when the mirror position changed by the angle just larger than 90°, it led to prevailing displacements across the slit.

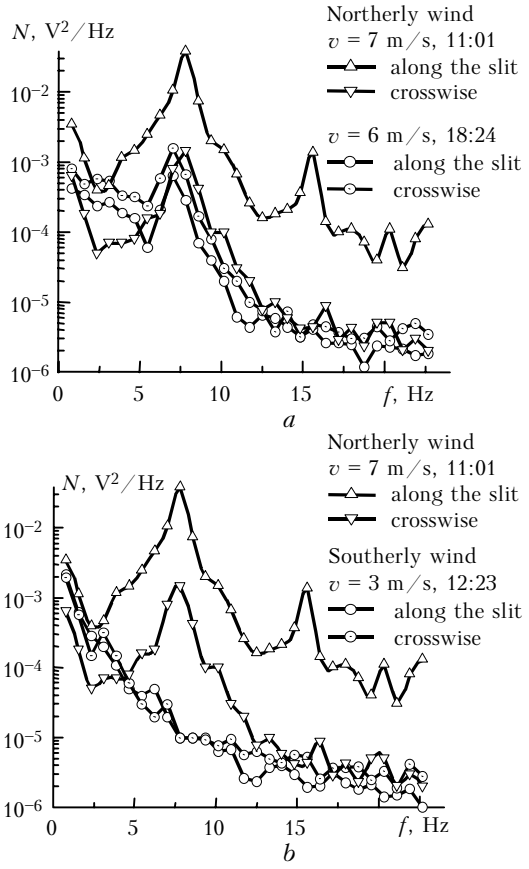

Fig. 5. Power spectra of the image displacement signals depending on the position of mirror of polar siderostat (*a*) and wind direction (*b*).

The variance of the image displacement signal at the second position of the mirror was far lower. This is likely connected with the fact that the wind direction in this case coincided with the axis of mirror fastening, while at the second position it was perpendicular to the mirror plane.

Figure 5*b* shows the power spectra of the image displacement signals recorded at the northerly and southerly wind. Unfortunately, meteorological conditions did not allow us to record signals at the same wind speed and at exactly the same local time. At the southerly wind the descending spectrum was observed, and at the northerly wind the spectrum had a maximum at the frequency of 7.8 Hz. The variance of the image jitter at the southerly wind was significantly lower than at the northerly wind.

The observed peculiarities of the spectra could make a basis for constructive solutions by the BSVT designers to improve the stability of the telescope mechanical mount.

Conclusion

The pilot version of the adaptive-optics system, which has been tested at the BSVT, provided for a sufficiently high degree of stabilization of a fragment of the solar disk image on the entrance slit of the spectrograph. This allowed the time of spectrum recording to be increased up to 300 s. However, for a continuously operating adaptive system at the BSVT, a new controlled mirror should be created with the size corresponding to the optical scheme of the system "telescope – spectrograph" (not decreasing the system aperture ratio), and the elements of the tracking system should be improved taking into account the revealed peculiarities in functioning of the pilot system.

Acknowledgments

We are thankful to our colleagues from the Institute of Solar-Terrestrial Physics for the opportunity of conducting experimental studies with their unique telescope and for the interest they showed in our work.

References

1. V.I. Skomorovsky and N.M. Firstova, Solar Physics **163**, 209–222 (1996).
2. L.V. Antoshkin, O.N. Emaleev, and V.P. Lukin, Prib. Tekhn. Eksp. No. 5, 211–212 (1988).
3. L.V. Antoshkin, N.N. Botygina, O.N. Emaleev, and V.P. Lukin, Atmos. Oceanic Opt. **8**, No. 10, 798–802 (1995).
4. L.V. Antoshkin, N.N. Botygina, L.N. Lavrinova, and V.A. Fedorov, Atmos. Oceanic Opt. **9**, No. 11, 975–976 (1996).
5. T. Berkefeld and A. Glindemann, Adaptive Optics, July 8–12, Maui, Hawaii; Technical Digest Series **13**, 206–208 (1996).